

Dense anomaly detection by robust learning on synthetic negative data

Matej Grcić, Petra Bevandić, Siniša Šegvić

*University of Zagreb, Faculty of Electrical Engineering and Computing
Unska 3, 10000 Zagreb, Croatia*

Abstract

Standard machine learning is unable to accommodate inputs which do not belong to the training distribution. The resulting models often give rise to confident incorrect predictions which may lead to devastating consequences. This problem is especially demanding in the context of dense prediction since input images may be partially anomalous. Previous work has addressed dense anomaly detection by discriminative training on mixed-content images. We extend this approach with synthetic negative patches which simultaneously achieve high inlier likelihood and uniform discriminative prediction. We generate synthetic negatives with normalizing flows due to their outstanding distribution coverage and capability to generate samples at different resolutions. We also propose to detect anomalies according to a principled information-theoretic criterion which can be consistently applied through training and inference. The resulting models set the new state of the art on standard benchmarks and datasets in spite of minimal computational overhead and refraining from auxiliary negative data.

Keywords: Dense anomaly detection, Semantic segmentation, Normalizing flow, out-of-distribution detection

1. Introduction

Modern transportation has experienced tremendous progress in the last decade. Nowadays, the vast majority of vehicles are shipped with some

Email address: `matej.grcic@fer.hr` (Matej Grcić)

level of driving assistance. The core ability towards further improvements in the field is to perceive and understand the environment around the ego-vehicle. Some of the related tasks are scene parsing [1], reconstruction [2], and semantic forecasting [3]. The basic form of scene understanding classifies every pixel into one of the K predefined classes, which corresponds to the task of semantic segmentation [1].

Recent semantic segmentation approaches [1, 4] are based on deep learning. A deep model for semantic segmentation maps the input RGB image $\mathbf{x}_{3 \times H \times W}$ into the corresponding prediction $\mathbf{y}_{K \times H \times W}$ where K denotes the number of known classes. Typically, the model parameters θ are obtained by gradient optimization of a supervised discriminative objective based on maximum likelihood. Recent approaches may produce high-fidelity segmentations of large images in real time even when inferring on a modest GPU [4]. However, standard learning is susceptible to overconfidence in incorrect predictions [5], which may make the model unusable in presence of domain shift [6]. This poses a huge threat for deep models deployed in the real world, especially in the field of autonomous driving.

We study the ability of deep models for natural image understanding to deal with out-of-distribution input. We desire to correctly segment the scene while simultaneously detecting anomalous objects which are unlike any scenery from the training dataset. Integration of dense anomaly detection and standard dense prediction results in dense open-set recognition. Such capability is especially important in road-driving scenarios where miss-detection of anomalous obstacles could cause accidents with serious consequences.

Previous approaches to dense anomaly detection rely on image resynthesis [7, 8, 9], Bayesian modeling [10, 11], recognition in the latent space [12, 13], or auxiliary negative training data [14, 15]. However, all these approaches have significant shortcomings. Image resynthesis and Bayesian approaches require extraordinary computational resources while being unable to deliver significant performance improvements. In any case, these methods are not suitable for real-time applications. Recognition in latent space [12] may be sensitive to feature collapse [16, 17] due to relying on a pretrained classifier. Reliance on auxiliary negative data may introduce several kinds of undesired bias such as overoptimistic performance on some test images. Moreover, appropriate negative data may be unavailable in some application areas.

This work addresses dense anomaly detection by encouraging a standard dense prediction model to emit uniform predictions in outliers [18]. We pro-

pose to perform the training on mixed-content images [15] which we craft by pasting synthetic negatives into inlier training images. The generative model for synthetic negatives is jointly trained to generate patches which give rise to uniform discriminative prediction and to assign high likelihood in inliers [18]. We argue that normalizing flows are better than GANs for the task at hand due to much better distribution coverage and more stable training. Additionally, normalizing flows can generate samples of variable spatial dimensions [19] which makes them especially suitable for mimicking anomalous objects of varying size.

This paper proposes several improvements over our preliminary report [20]. First, we show that Jensen-Shannon divergence is a criterion of choice both for training and inference. This is more principled than previous approaches which optimize KL divergence and perform inference according to max-softmax [18, 14]. Second, we propose two stage training in order to discourage overfitting of the discriminative model to synthetic outliers. Together with several lesser improvements, these contributions achieve state-of-the-art performance on standard benchmarks for dense anomaly detection, despite abstaining from auxiliary negative data [15], image resynthesis [8, 7] and Bayesian modelling [10]. The proposed method can accurately detect anomalies at three times larger distances than the previous best result. Finally, our method has minimal overhead over the standard discriminative model, making it especially suitable for real-time applications.

2. Related work

There are several computer vision tasks which require anomaly detection. In the simplest case we are interested whether a given image is an inlier or an outlier [21] (section 2.1). In practice, this often has to be integrated with the primary recognition task [22]. The resulting open-set classifiers produce predictions over a set of K known classes and one unknown class (section 2.2). Things get more complicated in the case of dense prediction where we have to deal with outlier objects in inlier scenes [15, 12, 8] (section 2.3).

The simplest approach to anomaly detection is to look at the likelihood produced by a generative model fitted to the training data. However, today we know that such approach is neither simple nor straight-forward [23]. Still, generative models can be useful in less obvious approaches to anomaly detection [18]. Generative flows are especially interesting in this context due

to outstanding distribution coverage and capability to generate samples at different resolutions (subsection 2.4).

2.1. Out-of-distribution detection

Out-of-distribution (OOD) detection [21] is a binary classification task which discriminates samples into inliers and outliers. In-distribution samples, also known as inliers, are generated by the same generative process as the training data. Contrary, outliers are generated by a generative process which is disjoint from the training distribution [23]. OOD detection is typically carried out according to scoring function $s_\delta : [0, 1]^{3 \times H \times W} \rightarrow \mathcal{R}$ which assigns the scalar score to each test sample. We detect anomalies by thresholding the anomaly score.

Early scoring functions utilize maximal softmax probability [21]. Calibration of such max-softmax detector can be further improved by utilizing anti-adversarial perturbations [24] or auxiliary negative data [18]. However, this approach may be unsuitable for atypical domains which are not represented in any of the large image datasets (e.g: medical, astronomical, and microscopic imagery). Additionally, we can not get rid of the doubt that experimental performance may be biased towards the particular negative dataset.

There are several prior approaches towards replacing real negatives with synthetic ones [18, 25]. A seminal approach [18] proposes cooperative training of a GAN generator and a standard classifier. The classifier loss requires uniform predictions in generated samples and thus encourages the generator to yield samples at the distribution border. This idea can be carried out without a separate generative model, by leveraging Langevin sampling [25]. However, adapting these approaches for dense prediction is neither straightforward nor trivial.

2.2. Open-set recognition

Open-set recognition integrates OOD detection with the standard classification [22]. These models discourage excessive generalization for K known classes and thus distinguish them from the remaining visual content of the open world. Many approaches address this goal by rejecting known classes in input samples recognized as outliers [26, 15, 12, 27].

A major problem for this task and OOD detection in general is that outliers and inliers may be indistinguishable in the feature space [17]. Feature collapse [16] can be alleviated by forcing the model to learn more informative

features. This can be implemented by supplying auxiliary self-supervised loss [17, 28] as well as by training on negative data which can be sourced from real datasets [14, 29, 15] or sampled from generative models [18, 20]

2.3. Dense open-set recognition

Dense open-set recognition has a great potential for improving visual perception in road-driving scenarios. The resulting models strive to detect unknown hazards while correctly segmenting the rest of the scene.

A principled Bayesian approach to dense anomaly detection measures epistemic uncertainty [10]. High epistemic uncertainty indicates insufficient knowledge about the model parameters [10]. Hence it may detect circumstances which were unobserved during the training. Alternatively, [12] estimates the likelihood to detect anomalies in feature space.

Several approaches to dense open-set recognition train on auxiliary negative data. This idea requires two implementation details [15]. First, the training has to be conducted on mixed-content images obtained by pasting negative patches into positive training examples. If this guideline is not observed, the trained model would be unable to locate the borders between inliers and outliers during inference. Second, the negative dataset should be as broad as possible (eg. ImageNet, ADE20k or COCO) in order to cover a large portion of the background distribution. This will likely introduce some inlier content into negative images, however the resulting noise can be alleviated by careful batch composition. The training can be implemented through a separate OOD head [15] or by maximizing softmax entropy in negative pixels [13]. Recent work shows that anomaly detector can also be trained on instance classes of an auxiliary semantic segmentation dataset [13].

Another line of work resynthesise the input scene using a conditional generative model [7, 8, 30]. Dissimilarity between the input and the resynthesized image gives rise to competitive OOD detection. Still, resynthesis requires significant computational overhead which limits real-world applications. A related approach [31] utilizes a parallel upsampling path for input reconstruction. This improves inference speed with respect to generative resynthesis approaches, but fails to correctly recreate cluttered scenes.

2.4. Generative modeling

The main goal of generative modeling is to approximate implicit distribution of the training data with a statistical model. Early approaches

consider unnormalized distributions [32] which require complex training procedures based on MCMC sample generation. Alternatively, the distribution can be autoregressively factorized [33], which allows likelihood estimation and powerful but slow sample generation. Both of these two approaches are unsuitable for generating synthetic negatives due to slow sampling.

VAEs [34] use a factorized variational approximation of the latent representation, which allows to learn a lower bound of the likelihood. However, such training requires storing both the encoder and the decoder in the GPU memory. This makes VAEs unsuitable for joint training with a dense prediction model, since the latter requires large batches and large crops [35]. Orthogonally, GANs [36] ignore the factorization of the likelihood. Instead, the generator network learns to mimic the dataset samples by competing in a minimax game. However, the produced samples do not span the entire support of the training distribution [37] which makes GANs unsuitable for our task.

Contrary to previous approaches, normalizing flows [19] model the likelihood by a bijective mapping towards a predefined latent distribution $p(\mathbf{z})$, typically a fully factorized Gaussian. Given a diffeomorphism f_γ , the likelihood is defined according to the change of variables formula:

$$p_\gamma(\mathbf{x}) = p(\mathbf{z}) \left| \det \frac{\partial \mathbf{z}}{\partial \mathbf{x}} \right|, \quad \mathbf{z} = f_\gamma(\mathbf{x}). \quad (1)$$

This approach requires computation of the Jacobian determinant ($\det \frac{\partial \mathbf{z}}{\partial \mathbf{x}}$). Therefore, a great emphasis is placed on the design of transformations with tractable determinant computation and efficient inverse. This setup is further improved by introducing skip connections which increase capacity and improve convergence speed [38].

A trained normalizing flow f_γ can be sampled in two steps. First, we sample the latent distribution to obtain the latent tensor \mathbf{z} . Second, we recover the sample through the inverse transformation $\mathbf{x} = f_\gamma^{-1}(\mathbf{z})$. Since f is a bijection, both the latent representation and the generated image have the same dimensionality ($\mathcal{R}^{3 \times H \times W} \rightarrow [0, 1]^{3 \times H \times W}$). This property is especially useful for generating synthetic negatives since it allows to train and sample the model on different resolutions [19].

3. Dense anomaly detection with NFlowJS

We train dense anomaly detection on mixed-content images [15] obtained by pasting artificial negatives into regular training images. We propose to generate such negatives by a jointly trained normalizing flow (section 3.1). We train our models to recognize outliers according to a principled information-theoretic criterion (section 3.2), and use the same criterion to express the anomaly score which we use for inference (section 3.3).

3.1. Generating anomalies by a jointly trained normalizing flow

We train our discriminative model by minimizing cross-entropy over inliers ($\mathbf{s}^{ij} = 0$) and maximizing prediction uncertainty in pasted negatives ($\mathbf{s}^{ij} = 1$) [14, 18, 29]:

$$L(\theta) = \sum_{i,j}^{H,W} -(1 - \mathbf{s}^{ij}) \cdot \ln p_{\theta}(\mathbf{y}^{ij} | \mathbf{x}') + \lambda \cdot \mathbf{s}^{ij} \cdot L_{\text{neg}}^{ij}(\theta). \quad (2)$$

We sample a randomly sized negative patch \mathbf{x}^- from a jointly trained normalizing flow f_{γ} . We assemble a mixed-content training image \mathbf{x}' by pasting \mathbf{x}^- atop an inlier training image \mathbf{x}^+ :

$$\mathbf{x}' = (\mathbf{1} - \mathbf{s}) \cdot \mathbf{x}^+ + \text{pad}(\mathbf{x}^-, \mathbf{s}) \quad \text{where } \mathbf{x}^- = f_{\gamma}^{-1}(\mathbf{z}), \quad \mathbf{z} \sim \mathcal{N}(0, \mathbf{I}). \quad (3)$$

The negative patch is pasted on a random location. The outlier mask \mathbf{s} has ones at the randomly selected pasting locations and zeros elsewhere. The synthetic outlier \mathbf{x}^- is zero-padded in order to allow pasting by elementwise addition.

We jointly train the normalizing flow alongside the primary discriminative model (cf. Figure 1) in order to satisfy two opposing criteria. First, the generated samples should yield uniform predictive distribution at the output of the discriminative model. This moves the generative distribution away from the inliers. Second, the normalizing flow should maximize the likelihood of inlier patches. This moves the generative distribution towards the inliers. Thus, such training encourages generation of synthetic samples at the boundary of the training distribution and incorporates outlier awareness within the primary discriminative model [18]. The joint training procedure minimizes the following loss:

$$L(\theta, \gamma) = L_{\text{gen}}(\gamma) + \sum_{i,j}^{H,W} (1 - \mathbf{s}^{ij}) \cdot L_{\text{cls}}^{ij}(\theta) + \lambda \cdot \mathbf{s}^{ij} \cdot L_{\text{neg}}^{ij}(\theta, \gamma). \quad (4)$$

L_{gen} is the negative log-likelihood of the inlier patch which we replace by the synthetic outlier. L_{cls} is the standard discriminative loss. We scrutinize L_{neg} in the following subsection.

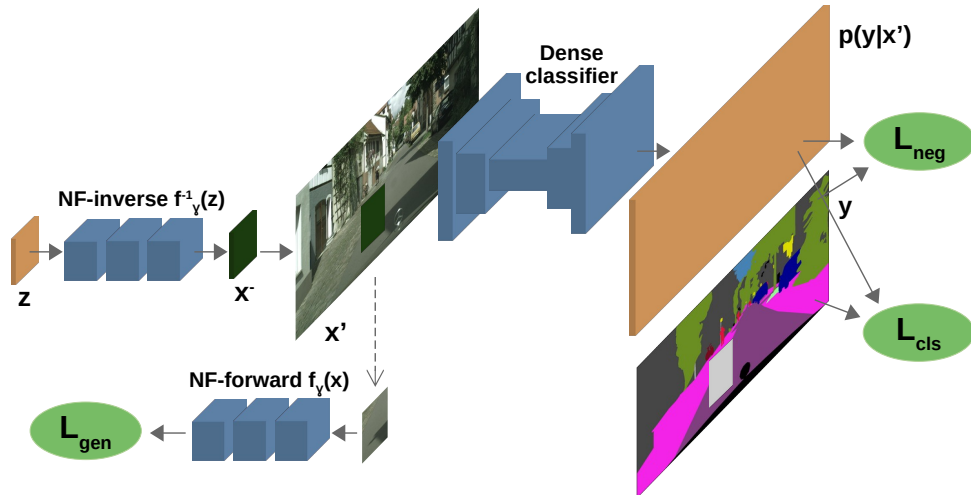


Figure 1: The proposed training setup. The normalizing flow generates the synthetic negative patch x^- which we paste atop the raw inlier image x^+ . The resulting mixed-content image x' is fed to the dense classifier which is trained to discriminate inlier pixels (L_{cls}) and to raise uniform predictions in negative pixels (L_{neg}). This formulation enables gradient flow from L_{neg} to the normalizing flow while maximizing the likelihood (L_{gen}) of inlier patches. Best viewed in color.

3.2. Robust loss in negative pixels

The loss L_{neg} has been often designed as KL-divergence between the uniform distribution and the model’s predictive distribution [18, 21, 29]. However, synthetic anomalies may contain parts which look alike chunks of inlier scenes. Discriminative predictions in such pixels are confident, which is strongly penalized by the KL-divergence. Such loss teaches the discriminative model to reduce the confidence in inlier content, and therefore triggers frequent false-positive responses of anomaly detector. Hence, we search the set of f-divergences for a more robust loss function.

Figure 2 (left) shows loss values for various f-divergences in the two-class setup. We observe that Jensen-Shannon divergence mildly penalizes high confidence predictions, which makes it a suitable candidate for our loss.

Figure 2 (right) shows a histogram of per-pixel losses which shows that JS-divergence offers robust penalisation in a realistic setup. Note that other f-divergences such as Pearson or Hellinger divergence are even more rigorous than the KL-divergence.

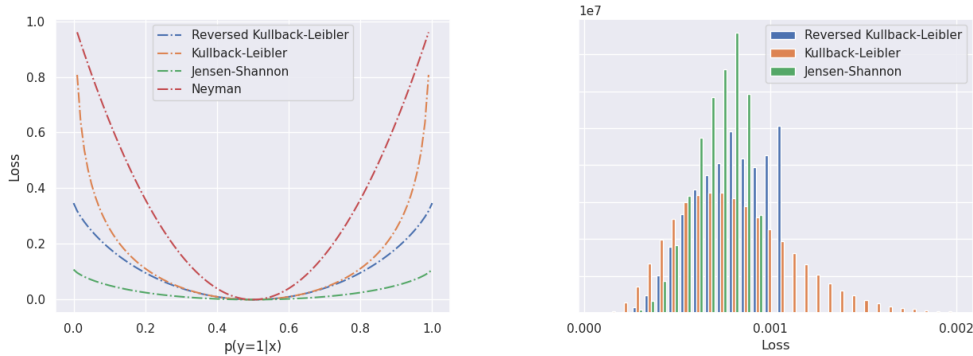


Figure 2: Left: f -divergences in the two-class setting. Right: Histograms of λL_{neg} in synthetic negatives at the beginning of the joint training on traffic datasets. The modulation factors λ have been separately validated for each of the three choices of L_{neg} . Jensen-Shannon divergence produces a more uniform learning signal than other f -divergences. Best viewed in color.

3.3. Inference with divergence-based scoring

Contrary to all existing designs, we propose to perform inference by aligning the scoring function with the training objective. Figure 3 illustrates the resulting dense open-set recognition method. The input image is fed into the discriminative model. The produced logits are fed into two branches. The top branch delivers closed-set predictions through arg-max. The bottom branch recovers the dense anomaly map through temperature scaling, softmax and JS divergence with respect to the uniform distribution. The two branches are fused into the final open-set segmentation map. The anomaly map overrides the closed-set prediction wherever the anomaly score exceeds a dataset-wide threshold.

We use temperature scaling [5] since it reduces the relative anomaly score of distributions with two dominant logits compared to distributions with homogeneous non-maximum logits. This discourages false positive OOD responses at semantic borders. We use the same temperature $T=2$ in all experiments which compare our performance with respect to previous methods.

Note that our inference is very fast since we use our generative model only to simulate anomalies during training. This is different from image resynthesis approaches where the generative model has to be used both during training and inference.

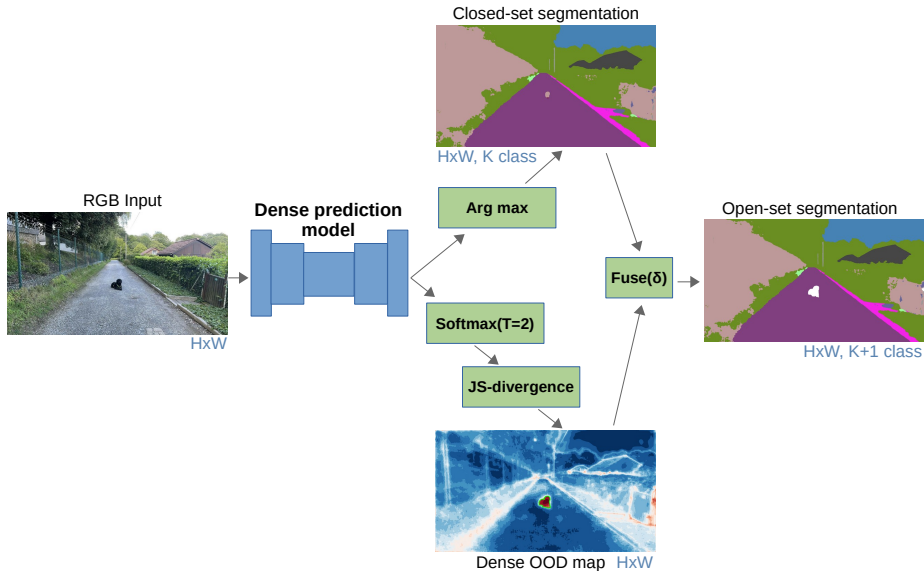


Figure 3: Proposed open-set inference. First, we perform inference with the primary dense prediction model. We recover the OOD map according to our divergence-based score (JSD). Closed-set predictions are overridden (white pixels in the final open-set output) wherever the OOD score exceeds the threshold δ . Best viewed in color.

4. Experimental setup

This section describes our experimental setup for dense anomaly detection. We first review the datasets which we use in our experiments. Subsequently, we describe the metrics which we use to evaluate the performance of our algorithms and compare them with the state of the art. Finally, we describe details of our training setup.

4.1. Benchmarks and Datasets

Benchmarking anomaly detection performance in road driving scenarios has experienced significant progress in recent years. Early approach [15]

pasted anomalies at a random position atop a road driving scene (cf. Figure 4, left). This was further improved by a more advanced pasting strategy which adapts shadows and lighting [12] (cf. Figure 4, center). Recent datasets avoid object pasting. Instead, they use real images in which the anomalies are fully-aligned with the environment [39] (cf. Figure 4, right). In parallel, significant effort has been invested into artificial datasets by leveraging simulated environments [40]. A simulated environment provides more freedom in insertion and manipulation of anomalies.

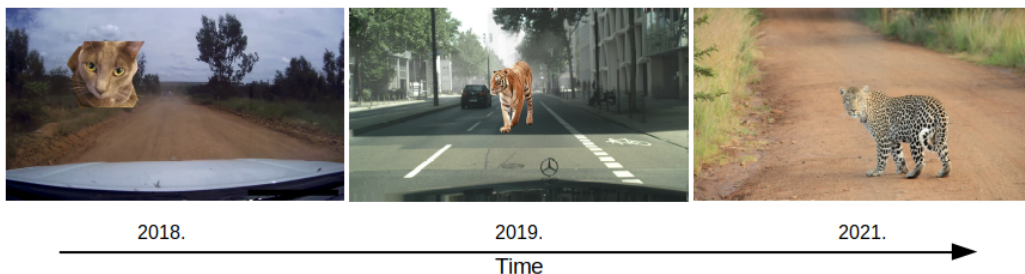


Figure 4: Advancement of dense anomaly detection datasets through time. Early approaches pasted object to random locations [15]. This was further improved by carefully choosing pasting locations, and several kinds of postprocessing [12]. Recent work ensures that anomalies match the environment by selecting adequate real-world scenes [39]. Best viewed in color.

WD-Pascal¹ [15] is an anomaly detection dataset created by pasting Pascal VOC objects into WildDash [6] images. WildDash images are challenging to segment due to difficult scenarios they capture. The resulting dataset allows to evaluate anomaly detection in demanding conditions. However, the random pasting policy disturbs the scene as shown in Figure 4 (left). Consequently, there is a possibility that such anomalies may be easier to detect.

Fishyscapes [12] evaluates model’s ability to detect anomalies in urban driving scenarios. The benchmark consists of two datasets: FS LostAndFound and FS Static. FS LostAndFound is a small subset of original LostAndFound [41] which contains small objects (e.g. toys, boxes or car parts that could fall off) on the roadway. FS Static contains Cityscapes validation images overlaid with Pascal VOC objects. The objects are positioned to mimic real world and further postprocessed to obtain smoother anomaly injection into the scene.

¹https://github.com/pb-brainiac/semseg_od

SegmentMeIfYouCan (SMIYC) [39] quantifies dense anomaly detection performance in multiple setups. The benchmark consists of three datasets: AnomalyTrack, ObstacleTrack and LostAndFound [41]. AnomalyTrack provides large anomalous objects which are fully aligned with the environment. For instance, they have a leopard in the savanna as shown in Fig. 4 (right). LostAndFound [41] tests detection of small hazardous objects (e.g. boxes, toys, car parts, etc.) in urban scenes. Finally, ObstacleTrack tests detection of small objects on various road types. Inconsistent road surfaces can trick detector causing high rate of false positives. Consequently, SMIYC benchmark provides a solid notion on anomaly segmentation performance of a model deployed in the wild.

StreetHazards [40] is a synthetic dataset created with the CARLA game engine. The dataset captures simulated urban environment with carefully inserted anomalous objects (e.g. a horse carriage or a helicopter parked on the road). Simulating anomalies in virtual environments is appealing due to high flexibility in positioning and appearance of anomalies. Moreover, simulating environments ensure low costs of data accumulation. Unfortunately, there is a notable quality mismatch between the simulated environment and the real world. Still, this approach has a great potential for evaluating various forms of anomaly detection.

4.2. Metrics

We measure anomaly segmentation performance using average precision (AP) and false-positive rate at true-positive rate of 95% (FPR_{95}) [12]. AP is well suited for measuring the anomaly detection performance since it emphasizes the detection of the minority class. A perfect classifier would have AP equal to one. Likewise, FPR_{95} is significant for real-world applications since high false-positive rates would imply a large number of human interventions in practical deployments and therefore severely diminish the practical value of an autonomous system.

4.3. Implementation details

All our models are based on the Ladder-DenseNet (LDN) [35] architecture due to its memory efficiency and near real-time performance on 2MPix. However, our framework can accommodate any other dense prediction architecture. All our experiments consist of two training stages. In both stages we utilize Cityscapes, Vistas and Wilddash 2 [6]. These three datasets contain

25 231 images. The images are resized to 1024 pixels (shorter edge), randomly flipped with the probability of 0.5, randomly resized in the interval $[0.5, 2]$, and randomly cropped to 768×768 pixels. We optimize our models with Adam optimizer. In the first stage we train for 25 epochs without synthetic anomalies. We use batch size 16 as validated in previous work [35]. The starting learning rate is set to 10^{-4} for the feature extractor and $4 \cdot 10^{-4}$ for the upsampling path. The learning rate is annealed according to a cosine schedule to the minimal value of 10^{-7} which would have been reached in the 50th epoch. In the second stage we train for 15 epochs on mixed content images, as described in Section 3.1. In this stage we use batch size 12 since this is the maximum which could fit to one GPU with 24 GB RAM. Note that we use gradient checkpointing [35]. The initial learning rate is set to $1 \cdot 10^{-5}$ for the upsampling path and $2.5 \cdot 10^{-6}$ for the backbone. Once more the learning rate is decayed according to the cosine schedule to the value of 10^{-7} . We set the hyperparameter λ to $3 \cdot 10^{-2}$. This value is chosen in a way that the performance on the primary segmentation task is not reduced.

Our normalizing flow generates rectangular anomalous patches with random spatial dimensions from the range $[16, 216]$. The flow is pretrained on random 64×64 crops from Vistas. We train the flow with the Adamax optimizer with learning rate set to 10^{-6} .

In the case of WD-Pascal dataset, we train our model only on Vistas in order to achieve a fair comparison with the previous work [15]. In the case of StreetHazards dataset, we train on the corresponding train subset for 80 epochs on inlier images and 40 epochs on mixed content images. In the case of Fishyscapes, we train exclusively on Cityscapes. We train for 150 epochs during stage 1 (inliers) and 50 epochs during stage 2 (mixed content). All other hyperparameters are kept constant across all experiments. Each experiment lasts for approximately 38 hours on a single NVIDIA RTX A5000.

5. Experimental evaluation

We evaluate our method on WD-Pascal, Fishyscapes, SegmentMeIfY-ouCan, and StreetHazards. We compare our performance with respect to contemporary methods which do not require the negative dataset nor image resynthesis. Still, we list all methods in our tables, so we can discuss our method in a broader context. We also analyze the sensitivity of our method with respect to the distance of the anomaly from the camera. Finally, we measure the computational overhead of our method with respect

to the baseline segmentation model, visualize our synthetic anomalies and ablate the proposed contributions.

5.1. Performance evaluation on WD-Pascal

Table 1 presents performance on WD-Pascal over 50 runs [15]. The bottom section compares our method with early approaches: MC dropout [10], ODIN [24], and max-softmax [21]. These approaches are not competitive with the current state-of-the-art.

The top section shows that training with auxiliary negative data can significantly improve the performance. However, our method closes the performance gap. It outperforms all other methods in FPR95 and AUROC metrics while achieving competitive AP.

| Method | Aux data | AP \uparrow | FPR ₉₅ \downarrow | AUROC \uparrow |
|----------------------|--------------|-----------------------|--------------------------------|-----------------------|
| OOD head [15] | \checkmark | 34.9 \pm 6.8 | 40.9 \pm 3.9 | 88.8 \pm 1.6 |
| Max softmax [15] | \checkmark | 33.8 \pm 5.1 | 35.5 \pm 3.4 | 91.1 \pm 1.0 |
| Void classifier [12] | \checkmark | 25.6 \pm 5.5 | 44.2 \pm 4.7 | 87.7 \pm 1.7 |
| MC Dropout 0.2 [10] | \times | 9.7 \pm 1.2 | 41.1 \pm 3.7 | 86.0 \pm 1.2 |
| MC Dropout 0.5 [10] | \times | 8.2 \pm 1.1 | 58.2 \pm 5.6 | 80.3 \pm 1.6 |
| ODIN [24] | \times | 6.0 \pm 0.5 | 53.7 \pm 7.0 | 79.9 \pm 1.5 |
| Max softmax [21] | \times | 5.0 \pm 0.5 | 48.8 \pm 4.7 | 78.7 \pm 1.5 |
| NFlowJS (ours) | \times | 30.2 \pm 4.1 | 32.3 \pm 5.9 | 92.3 \pm 1.3 |

Table 1: Performance evaluation on WD-Pascal [15]. Our method outperforms all other methods in FPR₉₅ and AUROC while offering competitive AP.

5.2. Performance evaluation on the Fishyscapes benchmark

Table 2 presents performance evaluation on the Fishyscapes benchmark. Once more, negative training data bring significant benefits. Nevertheless, our synthetic negative data succeed to tie-up the score on FS LostAnd-Found. Our method outperforms all previous methods in terms of FPR₉₅ while achieving the second best AP, by slightly underperforming only with respect to SynBoost which trains on real negative data.

The last section of the table shows a variant of our method which focuses on the ground during inference (GF stands for ground focus). We define the ground as a convex hull which covers all pixels predicted as the class road or the class sidewalk. This change entails a huge improvement in both metrics.

In the case of FS Static dataset, our method achieves the best FPR₉₅ and the second best AP among the methods which do not train on auxiliary data.

Training on auxiliary negative data may result in overoptimistic performance evaluation due to possible alignment between negative training data and actual anomalies in test images.

| Method | Requirements | | CS val mIoU | FS L&F | | FS Static | |
|---------------------|--------------|-------|----------------|-------------|-------------------|-------------|-------------------|
| | Aux data | Rsyn. | | AP | FPR ₉₅ | AP | FPR ₉₅ |
| SynBoost [7] | ✓ | ✓ | 81.4 | 43.2 | 15.8 | 72.6 | 18.8 |
| Prior Entropy [11] | ✓ | ✗ | 70.5 | 34.3 | 47.4 | 31.3 | 84.6 |
| OOD Head [15] | ✓ | ✗ | 79.6 | 31.3 | 19.0 | 96.8 | 0.3 |
| Void Class [12] | ✓ | ✗ | 70.4 | 10.3 | 22.1 | 45.0 | 19.4 |
| Image Resyn. [8] | ✗ | ✓ | 81.4 | 5.7 | 48.1 | 29.6 | 27.1 |
| Mutual Inform. [10] | ✗ | ✗ | 73.8 | 9.8 | 38.5 | 48.7 | 15.5 |
| Embed. Dens. [12] | ✗ | ✗ | 80.3 | 4.3 | 47.2 | 62.1 | 17.4 |
| Max softmax [21] | ✗ | ✗ | 80.3 | 1.8 | 44.9 | 12.9 | 39.8 |
| Softmax ent. [12] | ✗ | ✗ | 80.3 | 2.9 | 44.8 | 15.4 | 39.8 |
| SML [42] | ✗ | ✗ | - | 31.7 | 21.9 | 52.1 | 20.5 |
| NFlowJS (ours) | ✗ | ✗ | 77.4 | 39.4 | 9.0 | 52.1 | 15.4 |
| NFlowJS + GF (ours) | ✗ | ✗ | 77.4 | 69.4 | 2.0 | - | - |

Table 2: Results on the Fishyscapes benchmark. On FS L&F our method yields the best FPR₉₅ and the second best AP. On FS Static our method achieves the best FPR₉₅ and the second best AP among methods which do not use the negative data.

5.3. Performance evaluation on SegmentMeIfYouCan

Table 3 presents performance evaluation on SMIYC benchmark. Our method outperforms all previous methods which use image resynthesis [8, 9, 7], partial image reconstruction [31] or auxiliary data utilization [12].

Our method achieves very low FPR₉₅ (less than 1%) on ObstacleTrack and LostAndFound-noKnown. This is especially important for real-world applications where a high incidence of false positives may make the anomaly detection useless. Note that ObstacleTrack includes small anomalies in front of a variety of road surfaces, which makes it extremely hard not to misclassify road parts as anomalies. Moreover, this dataset includes low-visibility images captured at dusk and other challenging evaluation setups. More detailed performance evaluation on SMIYC benchmark is available in Appendix A.

Figure 5 shows the performance of the proposed method on two sequences of images from SMIYC LostAndFound dataset. Road groundtruth is designated in gray and the predicted anomaly in yellow. The top sequence contains an anomalous object which changes position through time. The bottom sequence contains multiple anomalous objects. Our method succeeds to detect

| Method | Aux data | Img rsyf. | AnomalyTrack | | ObstacleTrack | | LAF-noKnown | |
|----------------------|----------|-----------|--------------|-------------------|---------------|-------------------|-------------|-------------------|
| | | | AP | FPR ₉₅ | AP | FPR ₉₅ | AP | FPR ₉₅ |
| SynBoost [7] | ✓ | ✓ | 56.4 | 61.9 | 71.3 | 3.2 | 81.7 | 4.6 |
| Void Classifier [12] | ✓ | ✗ | 36.6 | 63.5 | 10.4 | 41.5 | 4.8 | 47.0 |
| Image Resyn. [8] | ✗ | ✓ | 52.3 | 25.9 | 37.7 | 4.7 | 57.1 | 8.8 |
| Road Inpaint. [9] | ✗ | ✓ | - | - | 54.1 | 47.1 | 82.9 | 35.8 |
| Max softmax [21] | ✗ | ✗ | 28.0 | 72.1 | 15.7 | 16.6 | 30.1 | 33.2 |
| MC Dropout [10] | ✗ | ✗ | 28.9 | 69.5 | 4.9 | 50.3 | 36.8 | 35.6 |
| ODIN [24] | ✗ | ✗ | 33.1 | 71.7 | 22.1 | 15.3 | 52.9 | 30.0 |
| Embed. Dens. [12] | ✗ | ✗ | 37.5 | 70.8 | 0.8 | 46.4 | 61.7 | 10.4 |
| JSRNet [31] | ✗ | ✗ | 33.6 | 43.9 | 28.1 | 28.9 | 74.2 | 6.6 |
| NFlowJS (ours) | ✗ | ✗ | 56.9 | 34.7 | 85.5 | 0.4 | 89.3 | 0.7 |

Table 3: Anomaly detection performance on SMIYC. We outperform all other methods. Our method has low FPR which makes it especially suitable for real-world applications.

a toy car and cardboard boxes even though no such objects were present during the training.



Figure 5: Anomaly detection on LostAndFound dataset. Our method can detect anomalies at different distances from the camera (top) as well as multiple anomalies in one image (bottom). Road groundtruth is designated in gray and the predicted anomaly in yellow. Best viewed in color.

Figure 6 shows performance of our method in two night scenes with over-exposure due to car headlights. We show our dense anomaly score in the second column. The third column shows the fused open-set segmentation map with anomalous pixels designated in white.

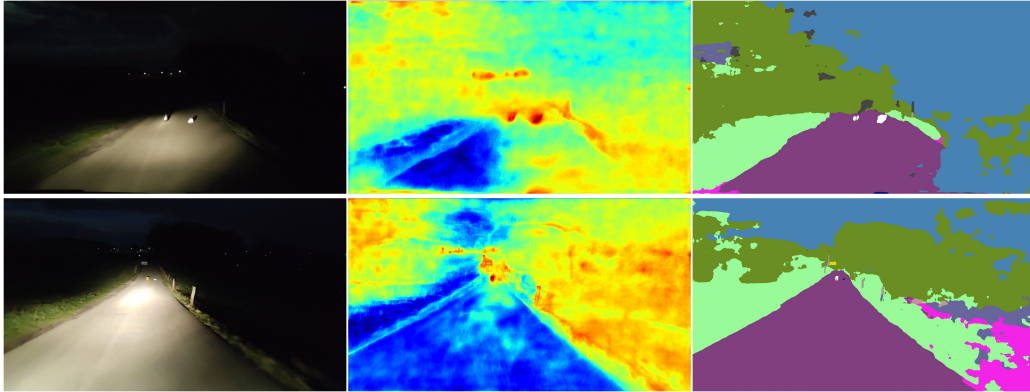


Figure 6: Anomaly detection in two night scenes from SMIYC-ObstacleTrack. The first column shows input images. The second column shows our dense anomaly scores. The third column shows the fused open-set segmentation map. Best viewed in color.

5.4. Performance evaluation on StreetHazards

Table 4 presents performance evaluation on StreetHazards. To the best of our knowledge, our method strongly outperforms all previous work. In particular, our method is better than methods based on conditional random fields [40], image resynthesis [30] and ensemble of networks formed by sampling weights distribution accumulated during the training [43].

| Method | Resyn. | mIoU \uparrow | AP \uparrow | FPR ₉₅ \downarrow | AUROC \uparrow |
|-------------------------|--------|-----------------|---------------|--------------------------------|------------------|
| SynthCP, $t=1$ [30] | ✓ | - | 8.1 | 46.0 | 81.9 |
| SynthCP, $t=0.999$ [30] | ✓ | - | 9.3 | 28.4 | 88.5 |
| Max softmax [21] | ✗ | 56.2 | 7.3 | 30.8 | 89.0 |
| Dropout [10][30] | ✗ | - | 7.5 | 79.4 | 69.9 |
| TRADI [43] | ✗ | - | 7.2 | 25.3 | 89.2 |
| MSP + CRF [40] | ✗ | - | 6.5 | 29.9 | 88.1 |
| S0+H [20] | ✗ | - | 12.7 | 25.2 | 91.7 |
| NFlowJS (ours) | ✗ | 56.8 | 28.4 | 14.9 | 95.7 |

Table 4: Performance on the StreetHazards [40] dataset. Our method outperforms all other methods in dense anomaly detection.

5.5. Sensitivity of anomaly detection to distance from the camera

We analyze sensitivity of anomaly detection to distance from the camera on the LostAndFound dataset which is included both in Fishyscapes and SMIYC. The used test set consists of 1203 images with the corresponding

pixel-level disparity maps based on which we compute the distances from the ego-vehicle. Due to limitations in the available disparity, we perform our analysis in range between 5 and 60 meters from the camera.

Figure 7 (left) shows histograms of inlier and outlier pixels. The figure shows that 62.5% of anomalous pixels are closer than 15 meters. Hence, the usual metrics are biased towards closer ranges. Indeed, as we further demonstrate, many methods fail to detect anomalies at longer distances.

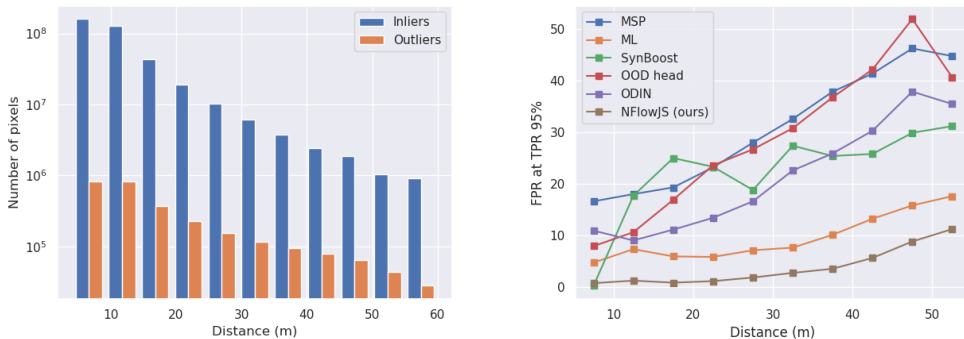


Figure 7: Left: Histogram of LostAndFound test set pixels. Right: Analysis of FPR at TPR of 95% at various distances from ego-vehicle. Best viewed in color.

We compare our method with the max-logit and max-softmax [21] baselines, ODIN [24], SynBoost [7] and OOD head [15] which trains on noisy negative data. Table 5 shows that many of these approaches produce a high number of false positives, even at small ranges, making them practically useless.

| Range (m) | 5-10 | 10-15 | 15-20 | 20-25 | 25-30 | 30-35 | 35-40 | 40-45 | 45-50 |
|----------------|------------|------------|------------|------------|------------|------------|------------|------------|------------|
| MSP [21] | 16.6 | 18.0 | 19.3 | 23.2 | 28.0 | 32.6 | 37.9 | 41.4 | 46.3 |
| ML [21] | 4.7 | 7.3 | 5.9 | 5.8 | 7.1 | 7.6 | 10.1 | 13.2 | 15.8 |
| SynBoost [7] | 0.2 | 17.7 | 25.0 | 23.3 | 18.8 | 27.4 | 25.4 | 25.8 | 29.9 |
| OOD head [15] | 7.9 | 10.6 | 16.9 | 23.6 | 26.7 | 30.8 | 36.8 | 42.2 | 52.0 |
| ODIN [24] | 10.9 | 9.0 | 11.1 | 13.4 | 16.6 | 22.6 | 25.9 | 30.3 | 37.9 |
| NFlowJS (ours) | 0.7 | 1.2 | 0.8 | 1.1 | 1.8 | 2.7 | 3.5 | 5.6 | 8.8 |

Table 5: Analysis of FPR at TPR of 95% at various distances from camera. Our method is a great candidate for real-world applications due to very low FPR rates at all distances.

Figure 7 (right) stratifies the relative performance of our method with respect to distance of the anomalies. Our method overcomes all previous

work by a wide margin at all distances except at close range (5-10m) where we perform comparably with SynBoost [7].

5.6. Inference speed

A convenient dense anomaly detector shouldn’t drastically increase already heavy computational burden of semantic segmentation. Hence, we measure computational overhead of our method and compare it with other approaches. We measure the inference speed on NVIDIA RTX 3090 for 1024×2048 inputs. Table 6 shows that SynBoost [7] and SynthCP [30] are not applicable for real-time inference since they require more than one second for inference. The baseline model LDN-121 [35] achieves near real-time inference for two megapixel images (46.5 ms, 21.5 FPS). ODIN [24] requires an additional forward-backward pass in order to recover the gradients of the loss with respect to the image. This results in a 3-fold slow-down with respect to the baseline. Similarly, MC Dropout [10] requires K forward passes for prediction with K MC samples. This results in 45.8 ms overhead when only 2 MC samples are used. Contrary, our approach increases the inference time for only 7.8 ms with respect to the baseline while outperforming all previous approaches. Note that the results for SynthCP are taken from [42].

| Method | Resynth. | Infer. Time (ms) | Overhead (ms) | FPS |
|--------------------------|----------|------------------|---------------|-------------|
| SynthCP [30] | ✓ | 146.9 | - | 6.8 |
| SynBoost [7] | ✓ | 1055.5 | - | < 1 |
| LDN-121 (Base) [35] | ✗ | 46.5 | - | 21.5 |
| Base + ODIN [24] | ✗ | 195.6 | 149.1 | 5.11 |
| Base + MC=2 Dropout [10] | ✗ | 92.3 | 45.8 | 10.83 |
| Base + NFlowJS (ours) | ✗ | 54.3 | 7.8 | 18.4 |

Table 6: Comparison of the inference speed for selected dense prediction approaches. Our method requires only 7.8ms overhead to produce the dense anomaly map, while the contemporary methods [7, 24, 10] are not applicable for real-time inference.

5.7. Visualization of synthetic outliers

Our normalizing flow generates samples at multiple resolutions with the same model. The generated samples have a limited variety when compared to a typical negative dataset such as ImageNet. Still, training with them greatly reduces overconfidence since the model is explicitly trained to discriminate between the known and the unknown. Figure 8 shows samples of a normalizing flow which was jointly trained as described in section 3.2.

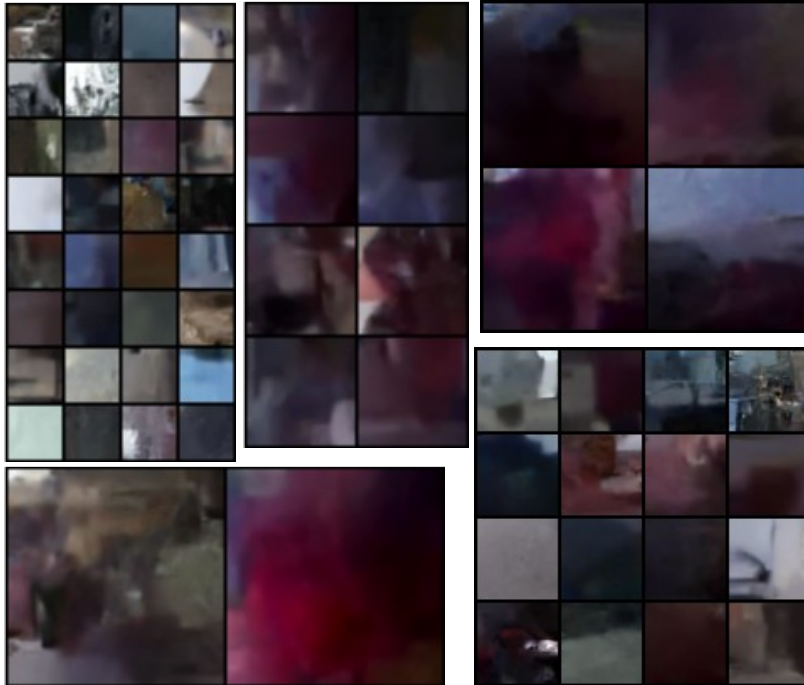


Figure 8: Samples of our generative model DenseFlow-25-6 which is jointly trained with our open-set segmentation model as proposed in section 3.1.

5.8. Impacts of the loss function and anomaly score

Table 7 analyzes the impact of the loss function (L_{neg}) and the anomaly score (s_δ) in negative pixels on large (AnomalyTrack val) and small anomalies (ObstacleTrack val). We separately validated the modulation factor λ for each choice of the negative loss, as well as the temperature parameter. We use $T=10$ for max-softmax and $T=2$ for divergence-based scoring functions. We report average performance over last three epochs. Row 1 shows the standard setting where the loss function is KL divergence between the uniform distribution and the softmax output [18, 14] while the anomaly score is max-softmax. Row 2 features the KL divergence both as the loss function and the anomaly score. Row 3 features the reversed KL divergence. Minimizing the reversed divergence between the uniform distribution and the softmax distribution is equivalent to maximizing the softmax entropy. Rows 4 and 5 feature the JS divergence. We observe that the reverse KL divergence outperforms the standard setup in 3 out of 4 metrics. JS divergence sub-

stantially outperforms all alternatives both as the loss function (JSD-MSP vs KL-MSP) and as the anomaly score (JSD-JSD vs JSD-MSP and RKL-RKL). We explain this advantage with robust response in synthetic outliers which resemble inliers, as well as with improved consistency during training and scoring (cf. sections 3.2 and 3.3).

| # | Loss | $s(\mathbf{x})$ | AnomalyTrack-val | | ObstacleTrack-val | |
|---|------|-----------------|-------------------|-------------------|-------------------|-------------------|
| | | | AP | FPR ₉₅ | AP | FPR ₉₅ |
| 1 | KL | MSP | 57.5 ± 0.7 | 29.0 ± 1.7 | 95.1 ± 0.2 | 0.2 ± 0.1 |
| 2 | KL | KL | 55.7 ± 0.4 | 26.3 ± 1.3 | 94.3 ± 0.2 | 0.1 ± 0.0 |
| 3 | RKL | RKL | 57.0 ± 0.3 | 28.9 ± 0.3 | 94.4 ± 0.1 | 0.3 ± 0.0 |
| 4 | JSD | MSP | 63.0 ± 0.5 | 22.8 ± 0.7 | 96.1 ± 0.2 | 0.2 ± 0.0 |
| 5 | JSD | JSD | 63.3 ± 0.6 | 19.8 ± 0.8 | 95.8 ± 0.2 | 0.1 ± 0.0 |

Table 7: Analysis of the loss function in negative pixels. The loss function based on JS-divergence outperforms the standard KL-divergence loss (row 4 vs row 1). Detecting anomalies using JSD scoring outperforms the standard ad hoc criterion (row 5 vs row 4).

5.9. Impact of temperature scaling

Table 8 shows the impact of softmax recalibration to anomaly detection. The table shows the performance on SMIYC val with temperatures T=1, T=1.5 and T=2. We observe that temperature scaling significantly improves divergence-based scoring.

| # | Temperature | AnomalyTrack-val | | ObstacleTrack-val | |
|---|-------------|-------------------|-------------------|-------------------|-------------------|
| | | AP | FPR ₉₅ | AP | FPR ₉₅ |
| 1 | T=1 | 59.7 ± 0.5 | 40.0 ± 0.8 | 92.6 ± 0.3 | 1.1 ± 0.1 |
| 2 | T=1.5 | 62.7 ± 0.6 | 23.7 ± 0.9 | 95.3 ± 0.2 | 0.2 ± 0.0 |
| 3 | T=2 | 63.3 ± 0.6 | 19.8 ± 0.8 | 95.8 ± 0.2 | 0.1 ± 0.0 |

Table 8: Impact of the softmax recalibration on dense anomaly detection. Temperature scaling improves our divergence-based anomaly detector.

5.10. Impact of the generative model capacity

Table 9 compares two variants of our method which are configured with different normalizing flows. The first variant uses the standard RealNVP [19] while the second uses DenseFlow-25-6 [38]. DenseFlow leads to better estimation of the likelihood as measured by bits per dimension (BPD) [19]. The

table suggests that better alignment of the generative model with the training distribution leads to improved anomaly detection due to more realistic synthetic negative data.

| # | Flow | BPD ↓ | AnomalyTrack-val | | ObstacleTrack-val | |
|---|--------------|-------------|-------------------|-------------------|-------------------|-------------------|
| | | | AP | FPR ₉₅ | AP | FPR ₉₅ |
| 1 | RNVP [19] | 2.24 | 61.6 ± 1.0 | 20.7 ± 0.4 | 94.9 ± 0.2 | 0.2 ± 0.0 |
| 2 | DF-25-6 [38] | 2.04 | 63.3 ± 0.6 | 19.8 ± 0.8 | 95.8 ± 0.2 | 0.1 ± 0.0 |

Table 9: Impact of the generative model to the performance of our method. A normalizing flow with more capacity produces better synthetic anomalies.

6. Conclusion

We have presented a novel method for dense anomaly detection and open-set recognition. Our method trains a dense discriminative model on mixed-content images obtained by pasting synthetic negative patches into training images.

We produce synthetic negatives by sampling a generative model which is jointly trained to maximize the likelihood and to produce uniform predictions at the far end of the discriminative model. Such collaborative learning leads to conservative unknown-aware predictions which are suitable for anomaly detection and open-set recognition.

We extend the previous work with the following contributions. First, we replace the adversarial generative model (GAN) with a normalizing flow. We believe that the resulting improvement is caused by better coverage of the training distribution. Second, we adapt the collaborative training setup for dense prediction. Generative flows are especially well-suited for this task due to straightforward generation at different resolutions. Third, we propose to prevent overfitting of the discriminative model to synthetic anomalies by pre-training the normalizing flow and the discriminative model prior to joint training. Fourth, we propose to use JS divergence as a principled criterion for training the discriminative model with synthetic anomalies. We also show that the same criterion can be used as a competitive replacement for ad-hoc scoring functions such as max-softmax.

We have evaluated the proposed method on standard benchmarks and datasets for dense anomaly detection. The results indicate state of the art performance at 6 out of 7 evaluation datasets, substantial advantage with respect to all previous approaches that do not train on real negative data,

as well as a very low overhead with respect to the dense prediction baseline. Consequently, the proposed method is appropriate for real-time applications. Suitable avenues for future work include allowing our method to train on real negative data, and extending it to other dense prediction tasks.

Acknowledgements

The authors would like to thank Jakob Verbeek for suggesting normalizing flows as a suitable tool for generating synthetic anomalies. This work has been supported by Croatian Science Foundation (grant IP-2020-02-5851 ADEPT), European Regional Development Fund and Gideon Brothers ltd (KK.01.2.1.02.0119 A-Unit).

References

- [1] C. Farabet, C. Couprie, L. Najman, Y. LeCun, Learning hierarchical features for scene labeling, *IEEE Trans. Pattern Anal. Mach. Intell.* 35 (8) (2013) 1915–1929.
- [2] J. Zbontar, Y. LeCun, Stereo matching by training a convolutional neural network to compare image patches, *J. Mach. Learn. Res.* 17 (2016) 65:1–65:32.
- [3] P. Luc, C. Couprie, Y. LeCun, J. Verbeek, Predicting future instance segmentation by forecasting convolutional features, in: 15th European Conference on Computer Vision, ECCV, 2018.
- [4] M. Orsic, S. Segvic, Efficient semantic segmentation with pyramidal fusion, *Pattern Recognit.* 110 (2021) 107611. doi:10.1016/j.patcog.2020.107611.
- [5] C. Guo, G. Pleiss, Y. Sun, K. Q. Weinberger, On calibration of modern neural networks, in: 34th International Conference on Machine Learning, ICML, 2017.
- [6] O. Zendel, K. Honauer, M. Murschitz, D. Steininger, G. F. Dominguez, Wilddash - creating hazard-aware benchmarks, in: European Conference on Computer Vision (ECCV), 2018.
- [7] G. D. Biase, H. Blum, R. Siegwart, C. Cadena, Pixel-wise anomaly detection in complex driving scenes, in: Computer Vision and Pattern Recognition, CVPR, 2021.
- [8] K. Lis, K. K. Nakka, P. Fua, M. Salzmann, Detecting the unexpected via image resynthesis, in: International Conference on Computer Vision, ICCV, 2019.
- [9] K. Lis, S. Honari, P. Fua, M. Salzmann, Detecting road obstacles by erasing them, CoRR abs/2012.13633.
- [10] A. Kendall, Y. Gal, What uncertainties do we need in bayesian deep learning for computer vision?, in: Neural Information Processing Systems, 2017.

- [11] A. Malinin, M. J. F. Gales, Predictive uncertainty estimation via prior networks, in: Annual Conference on Neural Information Processing Systems, 2018.
- [12] H. Blum, P.-E. Sarlin, J. Nieto, R. Siegwart, C. Cadena, The fishyscapes benchmark: Measuring blind spots in semantic segmentation, *International Journal of Computer Vision* 129 (11) (2021) 3119–3135.
- [13] R. Chan, M. Rottmann, H. Gottschalk, Entropy maximization and meta classification for out-of-distribution detection in semantic segmentation, in: International Conference on Computer Vision, ICCV, 2021.
- [14] D. Hendrycks, M. Mazeika, T. G. Dietterich, Deep anomaly detection with outlier exposure, in: 7th International Conference on Learning Representations, ICLR 2019.
- [15] P. Bevandic, I. Kreso, M. Orsic, S. Segvic, Simultaneous semantic segmentation and outlier detection in presence of domain shift, in: 41st DAGM German Conference, DAGM GCPR 2019. doi:10.1007/978-3-030-33676-9_3.
- [16] J. van Amersfoort, L. Smith, A. Jesson, O. Key, Y. Gal, On feature collapse and deep kernel learning for single forward pass uncertainty, arXiv preprint arXiv:2102.11409.
- [17] P. Perera, V. I. Morariu, R. Jain, V. Manjunatha, C. Wigington, V. Ordonez, V. M. Patel, Generative-discriminative feature representations for open-set recognition, in: Computer Vision and Pattern Recognition, CVPR, 2020.
- [18] K. Lee, H. Lee, K. Lee, J. Shin, Training confidence-calibrated classifiers for detecting out-of-distribution samples, in: 6th International Conference on Learning Representations, ICLR 2018.
- [19] L. Dinh, J. Sohl-Dickstein, S. Bengio, Density estimation using real NVP, in: 5th International Conference on Learning Representations, ICLR 2017.
- [20] M. Grcić, P. Bevandić, S. Šegvić, Dense open-set recognition with synthetic outliers generated by real NVP, in: 16th International Joint Conference on Computer Vision, Imaging and Computer Graphics Theory and Applications, VISIGRAPP 2021.
- [21] D. Hendrycks, K. Gimpel, A baseline for detecting misclassified and out-of-distribution examples in neural networks, in: 5th International Conference on Learning Representations, ICLR 2017.
- [22] W. J. Scheirer, A. de Rezende Rocha, A. Sapkota, T. E. Boult, Toward open set recognition, *IEEE Transactions on Pattern Analysis and Machine Intelligence* 35 (7) (2013) 1757–1772. doi:10.1109/TPAMI.2012.256.
- [23] L. H. Zhang, M. Goldstein, R. Ranganath, Understanding failures in out-of-distribution detection with deep generative models, in: 38th International Conference on Machine Learning, ICML, 2021.

- [24] S. Liang, Y. Li, R. Srikant, Enhancing the reliability of out-of-distribution image detection in neural networks, in: 6th International Conference on Learning Representations, ICLR 2018.
- [25] Z. Zhao, L. Cao, K. Lin, Revealing distributional vulnerability of explicit discriminators by implicit generators, CoRR abs/2108.09976.
- [26] A. Bendale, T. E. Boult, Towards open set deep networks, in: IEEE Conference on Computer Vision and Pattern Recognition, CVPR, 2016.
- [27] H. Zhang, A. Li, J. Guo, Y. Guo, Hybrid models for open set recognition, in: 16th European Conference on Computer Vision ECCV, 2020.
- [28] X. Zhang, J. Mu, X. Zhang, H. Liu, L. Zong, Y. Li, Deep anomaly detection with self-supervised learning and adversarial training, Pattern Recognit. 121.
- [29] A. R. Dhamija, M. Günther, T. E. Boult, Reducing network agnostophobia, in: Annual Conference on Neural Information Processing Systems 2018, NeurIPS 2018.
- [30] Y. Xia, Y. Zhang, F. Liu, W. Shen, A. L. Yuille, Synthesize then compare: Detecting failures and anomalies for semantic segmentation, in: 16th European Conference on Computer Vision, ECCV, 2020.
- [31] T. Vojir, T. Šipka, R. Aljundi, N. Chumerin, D. O. Reino, J. Matas, Road anomaly detection by partial image reconstruction with segmentation coupling, in: International Conference on Computer Vision, ICCV, 2021.
- [32] R. Salakhutdinov, G. Hinton, Deep boltzmann machines, in: Twelfth International Conference on Artificial Intelligence and Statistics, PMLR, 2009.
- [33] A. Van Oord, N. Kalchbrenner, K. Kavukcuoglu, Pixel recurrent neural networks, in: International Conference on Machine Learning, PMLR, 2016.
- [34] D. P. Kingma, M. Welling, Auto-encoding variational bayes, in: 2nd International Conference on Learning Representations, ICLR, 2014.
- [35] I. Kreso, J. Krapac, S. Segvic, Efficient ladder-style densenets for semantic segmentation of large images, IEEE Trans. Intell. Transp. Syst. 22.
- [36] I. J. Goodfellow, J. Pouget-Abadie, M. Mirza, B. Xu, D. Warde-Farley, S. Ozair, A. C. Courville, Y. Bengio, Generative adversarial networks, Commun. ACM 63.
- [37] T. Lucas, K. Shmelkov, K. Alahari, C. Schmid, J. Verbeek, Adaptive density estimation for generative models, in: Neural Information Processing Systems, 2019.
- [38] M. Grečić, I. Grubišić, S. Šegvić, Densely connected normalizing flows, in: Neural Information Processing Systems, 2021.

- [39] R. Chan, K. Lis, S. Uhlemeyer, H. Blum, S. Honari, R. Siegwart, M. Salzmann, P. Fua, M. Rottmann, Segmentmeifyoucan: A benchmark for anomaly segmentation, CoRR abs/2104.14812.
- [40] D. Hendrycks, S. Basart, M. Mazeika, M. Mostajabi, J. Steinhardt, D. Song, Scaling out-of-distribution detection for real-world settings, arXiv preprint arXiv:1911.11132.
- [41] P. Pinggera, S. Ramos, S. Gehrig, U. Franke, C. Rother, R. Mester, Lost and found: detecting small road hazards for self-driving vehicles, in: International Conference on Intelligent Robots and Systems, IROS, 2016.
- [42] S. Jung, J. Lee, D. Gwak, S. Choi, J. Choo, Standardized max logits: A simple yet effective approach for identifying unexpected road obstacles in urban-scene segmentation, in: International Conference on Computer Vision, ICCV, 2021.
- [43] G. Franchi, A. Bursuc, E. Aldea, S. Duboisson, I. Bloch, TRADI: tracking deep neural network weight distributions, in: 16th European Conference on Computer Vision, ECCV, 2020.

Biography

Matej Grcić received an M.Sc.degree from the Faculty of Electrical Engineering and Computing in Zagreb. He finished the master study program in Computer Science in 2020. He is pursuing his Ph.D. degree at Uni-ZG FER. His research interests include generative modeling and open-world recognition.

Petra Bevandić received an M.Sc.degree from the Faculty of Electrical Engineering and Computing in Zagreb. She finished the master study program in Computer Science in 2014. She is pursuing his Ph.D. degree at Uni-ZG FER. Her research interests include robust and open-world recognition.

Siniša Šegvić received a Ph.D. degree in computer science from the University of Zagreb, Croatia. He was a post-doctoral researcher at IRISA Rennes and also at TU Graz. He is currently a full professor at Uni-ZG FER. His research interests focus on deep convolutional architectures for classification and dense prediction.

Appendix A. Extended SMIYC results

| Method | Aux data | Img rsyn. | Pixel Level | | Component Level | | |
|----------------------|----------|-----------|---------------|--------------------------------|--------------------|----------------|---------------|
| | | | AP \uparrow | FPR ₉₅ \downarrow | sIoU-gt \uparrow | PPV \uparrow | F1 \uparrow |
| SynBoost [7] | ✓ | ✓ | 56.4 | 61.9 | 34.7 | 17.8 | 10.0 |
| Void Classifier [12] | ✓ | ✗ | 36.6 | 63.5 | 21.1 | 22.1 | 6.5 |
| Maxim. Ent. [13] | ✓ | ✗ | 85.5 | 15.0 | 49.2 | 39.5 | 28.7 |
| Image Resyn. [8] | ✗ | ✓ | 52.3 | 25.9 | 39.7 | 11.0 | 12.5 |
| Max softmax [21] | ✗ | ✗ | 28.0 | 72.1 | 15.5 | 15.3 | 5.4 |
| MC Dropout [10] | ✗ | ✗ | 28.9 | 69.5 | 20.5 | 17.3 | 4.3 |
| ODIN [24] | ✗ | ✗ | 33.1 | 71.7 | 19.5 | 17.9 | 5.2 |
| Embed. Dens. [12] | ✗ | ✗ | 37.5 | 70.8 | 33.9 | 20.5 | 7.9 |
| JSRNet [31] | ✗ | ✗ | 33.6 | 43.9 | 20.2 | 29.3 | 13.7 |
| Ours | ✗ | ✗ | 56.9 | 34.7 | 36.9 | 18.0 | 14.9 |

Table A.10: Anomaly detection performance on SMIYC AnomalyTrack.

| Method | Aux data | Img rsyn. | Pixel Level | | Component Level | | |
|----------------------|----------|-----------|---------------|--------------------------------|--------------------|----------------|---------------|
| | | | AP \uparrow | FPR ₉₅ \downarrow | sIoU-gt \uparrow | PPV \uparrow | F1 \uparrow |
| SynBoost [7] | ✓ | ✓ | 71.3 | 3.2 | 44.3 | 41.8 | 37.6 |
| Void Classifier [12] | ✓ | ✗ | 10.4 | 41.5 | 6.3 | 20.3 | 5.4 |
| Maxim. Ent. [13] | ✓ | ✗ | 85.1 | 0.8 | 47.9 | 62.6 | 48.5 |
| Image Resyn. [8] | ✗ | ✓ | 37.7 | 4.7 | 16.6 | 20.5 | 8.4 |
| Road Inpaint [9] | ✗ | ✓ | 54.1 | 47.1 | 57.6 | 39.5 | 36.0 |
| Max softmax [21] | ✗ | ✗ | 15.7 | 16.6 | 19.7 | 15.9 | 6.3 |
| MC Dropout [10] | ✗ | ✗ | 4.9 | 50.3 | 5.5 | 5.8 | 1.1 |
| ODIN [24] | ✗ | ✗ | 22.1 | 15.3 | 21.6 | 18.5 | 9.4 |
| Embed. Dens. [12] | ✗ | ✗ | 0.8 | 46.4 | 35.6 | 2.9 | 2.3 |
| JSRNet [31] | ✗ | ✗ | 28.1 | 28.9 | 18.6 | 24.5 | 11.0 |
| Ours | ✗ | ✗ | 85.5 | 0.4 | 45.5 | 49.5 | 50.4 |

Table A.11: Anomaly detection performance on SMIYC ObstacleTrack.

| Method | Aux data | Img rsyn. | Pixel Level | | Component Level | | |
|----------------------|-------------|--------------|---------------|--------------------------------|--------------------|----------------|---------------|
| | | | AP \uparrow | FPR ₉₅ \downarrow | sIoU-gt \uparrow | PPV \uparrow | F1 \uparrow |
| SynBoost [7] | ✓ | ✓ | 81.7 | 4.6 | 36.8 | 72.3 | 48.7 |
| Void Classifier [12] | ✓ | ✗ | 4.8 | 47.0 | 1.8 | 35.1 | 1.9 |
| Maxim. Ent. [13] | ✓ | ✗ | 77.9 | 9.7 | 45.9 | 63.1 | 49.9 |
| Image Resyn. [8] | ✗ | ✓ | 57.1 | 8.8 | 27.2 | 30.7 | 19.2 |
| Road Inpaint [9] | ✗ | ✓ | 82.9 | 35.8 | 49.2 | 60.7 | 52.3 |
| Max softmax [21] | ✗ | ✗ | 30.1 | 33.2 | 14.2 | 62.2 | 10.3 |
| MC Dropout [10] | ✗ | ✗ | 36.8 | 35.6 | 17.4 | 34.7 | 13.0 |
| ODIN [24] | ✗ | ✗ | 52.9 | 30.0 | 39.8 | 49.3 | 34.5 |
| Embed. Dens. [12] | ✗ | ✗ | 61.7 | 10.4 | 37.8 | 35.2 | 27.6 |
| JSRNet [31] | ✗ | ✗ | 74.2 | 6.6 | 34.3 | 45.9 | 36.0 |
| NFlowJS (ours) | ✗ | ✗ | 89.3 | 0.7 | 54.6 | 59.7 | 61.8 |

Table A.12: Anomaly detection performance on SMIYC LostAndFound.